

# Polymer-Directed Nanocluster Synthesis: Control of Particle Size and Morphology

Rina Tannenbaum,<sup>\*,†</sup> Melissa Zubris,<sup>†</sup> Eugene P. Goldberg,<sup>‡</sup> Shimon Reich,<sup>§</sup> and Nily Dan<sup>\*,‡,⊥</sup>

*School of Materials Science and Engineering, Georgia Institute of Technology, Atlanta, Georgia 30332; Department of Materials Science and Engineering, University of Florida, Gainesville, Florida 32611; Department of Materials and Interfaces, Weizmann Institute of Science, Rehovot 76100, Israel; and Department of Chemical Engineering, Drexel University, Philadelphia, Pennsylvania 19104*

*Received August 16, 2004; Revised Manuscript Received March 6, 2005*

**ABSTRACT:** The ability to design nanomaterial characteristics requires exact control of particle structure due to the sensitive relationship between the material properties and the particle size and morphology. Borrowing nature's approach where biomineralization is controlled by macromolecules, synthetic polymeric matrices are used to guide the formation of stable, monodisperse iron oxide nanoparticles uniformly distributed in the polymeric matrix. Particle size, size distribution, and morphology are determined by the polymer–particle interactions and are independent of the chain molecular weight:  $\gamma$ -Fe<sub>2</sub>O<sub>3</sub> particles formed in strongly interacting polymeric media are small ( $\sim 10$ – $20$  nm) and pyramidal in shape, while those formed in weakly interacting media are larger ( $\sim 40$ – $60$  nm) and spherical. This synthesis method can be easily extended to a variety of inorganic nanoparticle chemistries, thereby enabling exact control over material properties.

## 1. Introduction

The properties of nanostructured materials are determined by the domain size and morphology.<sup>1</sup> Classical nucleation and growth processes tend to produce nanoparticles with a wide size distribution and little control over particle morphology.<sup>2</sup> The resulting heterogeneity in material properties limits the use of polydisperse nanoparticles in technologies such as photonic band-gap or quantum dots (e.g., refs 2–6). Developing new techniques for the controlled synthesis of monodisperse, stable (namely, flocculation resistant) populations of inorganic nanoparticles with easily tunable properties is, therefore, one of the great challenges to materials research today.<sup>7</sup>

In nature, the morphology and growth dynamics of inorganic biominerals are controlled by biopolymers (e.g., refs 8–10). Recent studies have shown that synthetic polymers in solutions can “cap” growing metal nanoparticles and affect their growth (e.g., refs 11 and 12). Here we develop this idea into a relatively universal methodology for the synthesis of inorganic nanoclusters, where the interfacial interactions between the growing nanoparticle and a homogeneous polymeric environment are used to select the particle properties. Specifically, conducting the particle formation in a polymeric melt allows control, *in a predictable way*, of particle size, size distribution, and morphology.

Quite surprisingly, nanoparticle properties are insensitive to the synthesis temperature and to polymer molecular weight, so that relatively short chains may be used to obtain the desired characteristics. Unlike nanoparticles synthesized in small molecule environments, particles formed in a polymeric matrix are

stabilized against flocculation by an adsorbed layer. If kept in the polymeric media, the result is a uniform nanocomposite of well-dispersed metal nanoparticles embedded in a polymeric matrix. If removed from the polymeric media through dissolution in a solvent, the result is sterically stabilized nanoparticles that resist aggregation.

To demonstrate the methodology, we focus on the decomposition of iron–carbonyl precursor to iron oxide nanoclusters ( $\gamma$ -Fe<sub>2</sub>O<sub>3</sub>) in several types of polymeric media. Iron oxides can appear in several stoichiometries and phases that display widely different magnetic properties, e.g., ferrimagnetic maghemite,  $\gamma$ -Fe<sub>2</sub>O<sub>3</sub>, and antiferromagnetic hematite,  $\alpha$ -Fe<sub>2</sub>O<sub>3</sub>.<sup>13,14</sup> Therefore, the use of iron oxide nanoparticles in applications such as magnetic recording media or cellular imaging requires exact control over the particles characteristics.<sup>15–17</sup> Current methods for the synthesis of  $\gamma$ -Fe<sub>2</sub>O<sub>3</sub> nanoparticles include sol–gel processes,<sup>18–20</sup> microemulsion templating,<sup>21,22</sup> or confinement in mesoporous media.<sup>23</sup> Although generally successful, these methods require the development of a templating medium (microemulsion, mesoporous scaffold) or specialized chemistries. In contrast, the synthesis process described here involves the simple mixing of iron pentacarbonyl (Fe(CO)<sub>5</sub>) suspensions with a polymer melt, followed by heating to moderate temperatures to initiate decomposition into iron oxide, as described in detail in this paper and elsewhere.<sup>24–26</sup> It should be noted that the synthesis temperature (which was varied between 70 and 143 °C) affected the particle growth rate, but not the equilibrium particle size.

## 2. Experimental Methods

**2.1. Preparation of Composite Films.** *General.* Measured masses of polymeric pellets were initially mixed into an appropriate solvent for 48 h at room temperature in a 100 mL glass-stoppered Erlenmeyer flask. The solvent was dried using molecular sieve pellets (Matheson, Coleman and Bell) prior to its use and stored under a nitrogen atmosphere. Iron

<sup>†</sup> Georgia Institute of Technology.

<sup>‡</sup> University of Florida.

<sup>§</sup> Weizmann Institute of Science.

<sup>⊥</sup> Drexel University.

\* Corresponding authors. E-mail: rina.tannenbaum@mse.gatech.edu; dan@coe.drexel.edu.

**Table 1. Summary of the Composition, Particle Size and Particle Size Distribution of the Iron Oxide Nanoclusters Produced in Various Polymer Matrices via the Decomposition of Fe(CO)<sub>5</sub> Precursor under Ambient Atmosphere and at Various Temperatures**

polymer composite system	particles formed	particle size (nm)
Fe(CO) <sub>5</sub> –PS	γ-Fe <sub>2</sub> O <sub>3</sub> α-FeO(OH) and α-Fe (trace)	67.2 ± 4.7 <sup>a</sup>
Fe(CO) <sub>5</sub> –PC	γ-Fe <sub>2</sub> O <sub>3</sub> α-FeO(OH) and α-Fe (trace)	10.8 ± 1.9
Fe(CO) <sub>5</sub> –PSF	γ-Fe <sub>2</sub> O <sub>3</sub> α-FeO(OH) and α-Fe (trace)	22.1 ± 3.1
Fe(CO) <sub>5</sub> –PMMA	γ-Fe <sub>2</sub> O <sub>3</sub> α-FeO(OH) and α-Fe (trace)	11.4 ± 1.9 <sup>a</sup>
Fe(CO) <sub>5</sub> –PVDF	γ-Fe <sub>2</sub> O <sub>3</sub> α-FeO(OH) and α-Fe (trace)	36.7 ± 4.0
Fe(CO) <sub>5</sub> –toluene	γ-Fe <sub>2</sub> O <sub>3</sub> α-FeO(OH) and α-Fe (trace)	270 ± 100

<sup>a</sup> For  $\bar{M}_w = 250\,000$  g/mol.

pentacarbonyl (Alfa Products, Thiokol/Ventron Division) was filtered through filter paper circles (Whatman 7.0 cm, qualitative 4) into a foil-covered test tube. One mL of the filtered Fe(CO)<sub>5</sub> was then added dropwise into the polymer solution. After mixing vigorously for approximately 5 min, the iron pentacarbonyl/polymer solution was film cast onto sheets of glass using a 0.005 in. or 0.020 in. steel doctor blade, and the solvent was allowed to evaporate. Thermal decompositions were carried out in a temperature-controlled vacuum oven with controlled atmosphere capability. The decomposition temperature (which was varied between 70 and 143 °C) was found to change system kinetics but did not affect the equilibrium particle size and size distribution. Since Fe(CO)<sub>5</sub> has a relatively high vapor pressure at room temperature, some of the original carbonyl was lost due to evaporation prior to decomposition. Therefore, all films were analyzed for iron content to determine the actual Fe(CO)<sub>5</sub> retained using the infrared absorption band (measured on Nicolet MX-1 and Nicolet Nexus 870 Fourier transform infrared spectrophotometers) at 1996 cm<sup>-1</sup> (carbonyl stretching). Further details may be found in the pertinent references.<sup>24–26</sup>

**Specific Systems.** 10 g of polycarbonate (LEXAN, 131-111,  $\bar{M}_w = 32\,200$  g/mol,  $d = 1.21$  g/cm<sup>3</sup>) was initially dissolved in 43.9 mL of methylene chloride (Fisher Reagent), 10 g of polysulfone (UDELL,  $\bar{M}_w = 30\,100$  g/mol,  $d = 1.24$  g/cm<sup>3</sup>) was dissolved in 41.5 mL of methylene chloride (Fisher Reagent), 5 g of polystyrene (Polyscience, Inc., different chain lengths as discussed in the text,  $d = 1.04$ – $1.05$  g/cm<sup>3</sup>) was dissolved in 30.0 mL of toluene (Fisher-Reagent), 5 g of PMMA (Polyscience, Inc., different chain lengths as discussed in the text,  $d = 1.17$ – $1.20$  g/cm<sup>3</sup>) was dissolved in 30.0 mL of toluene (Fisher-Reagent), and finally, 10.0 g of poly(vinylidene difluoride) pellets (Polyscience, Inc.,  $\bar{M}_w = 279\,000$  g/mol,  $d = 1.75$  g/cm<sup>3</sup>) was dissolved in 94.8 mL of *N,N*-dimethylformamide (Fisher Reagent).

**2.2. Particle Characterization.** Particle size and size distributions were measured by transmission electron microscopy using both TEM (Hitachi HF-2000, JEOL 2010, and JEOL model 200CX) and a high-resolution TEM (JEOL 4000EX). The operating voltage was 200 keV for all three microscopes. Electron diffraction patterns from a TEM field emission gun were used to study the composition and morphology of metallic particles. Two types of samples were examined for each system: (1) A 0.1% solution of polymer and Fe(CO)<sub>5</sub> solution (in the appropriate system-specific solvent) was applied to carbon-coated (100 Å thick) TEM grids, dried to evaporate the solvent, and then heated to the decomposition temperature. (2) Composite films were embedded in epoxy resin (Epon 812) and ultramicrotomed (LKB Ultratome) for TEM studies. Particle size, size distribution, and morphology were found to be independent of the sample preparation technique and are summarized in Table 1. The particles were characterized by both electron diffraction analysis and X-ray

diffraction. In all cases, the particles were polycrystalline and consisted of mainly γ-Fe<sub>2</sub>O<sub>3</sub> (>90%), α-FeO(OH), and traces of α-Fe, as shown in Table 1 as well.

**2.3. Theoretical Model.** As discussed above, the effect of a polymeric environment of the synthesis of an inorganic particle is not well understood. We develop here a scaling model to describe, qualitatively, the effect of a polymeric matrix on the formation of an inorganic particle.

The free energy of an adsorbed chain is composed of two terms:<sup>27,28</sup> one scaling as  $Na^2/L^2$ , where  $N$  is the chain length,  $a$  is the segment size, and  $L$  is the adsorbed layer thickness, and the interaction energy with the particle, which is given by  $-4\pi\epsilon r^2/n$ , where  $\epsilon$  is the reduced interfacial energy (per unit area),  $r$  the particle radius, and  $n$  the number of adsorbed chains. The volume fraction of the adsorbed chains in the adsorbed layer,  $x$ , is not unity—despite the fact that the synthesis is done in the melt. This is because there is interpenetration of nonadsorbing chains into the layer. Thus,  $n$ ,  $L$ , and  $x$  are related through a geometric relationship (e.g., ref 25).

The number of metal particles is proportional to the metal volume fraction,  $\phi$ , divided by the volume of a single particle ( $\sim r^3$ ). The overall system energy scales, therefore<sup>27,28</sup> (neglecting the numerical coefficients), as  $\phi[n(Na^2/L^2) - \epsilon r^2 + \ln \phi]/r^3$ . Minimization of the free energy with respect to  $r$ ,  $x$ , and  $n$  leads to the relationship described below in the text.

The interactions between two nanoparticles are combined of two competing forces: van der Waals,<sup>29</sup> which favors aggregation, and the deformation energy of the adsorbed chains,<sup>25</sup> which resists particles coming together:  $p \approx (-A/D^2) + (nL^2/r^{*2}D^2)$ , where  $p$  is the interaction energy (per unit area),  $A$  the Hamaker constant,  $n$  the number of adsorbed chains per particle,  $L$  the adsorbed layer thickness (at equilibrium),  $r^*$  the equilibrium particle radius, and  $D$  the distance between particle edges, assuming that  $D \ll r^*$ . We see that, if the expression in parentheses is positive, the net interaction between particles will be repulsive. If it is negative, the interaction will be attractive and they will flocculate. Substituting the equilibrium values obtained for  $r^*$ ,  $n$ , and  $L$  we get the relationship described below.

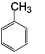
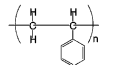
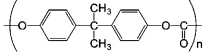
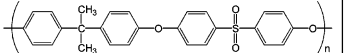
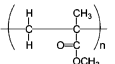
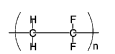
### 3. Results and Discussion

We first examine the effect of the polymer environment on cluster properties by comparing iron oxide clusters formed in a polystyrene melt (PS) to those formed using a similar procedure in toluene, a small molecule solvent. Although toluene and styrene are chemically similar (Table 2), we find that the average diameter of clusters in polystyrene is  $67 \pm 4$  nm, while those formed in toluene are of order  $270 \pm 100$  nm. The latter is in qualitative agreement with, for example, Kimata et al.,<sup>30</sup> who used hydrolysis of iron tri-*n*-butoxide in an octanol/acetonitrile solution to form (γ-Fe<sub>2</sub>O<sub>3</sub>) particles of order 0.5 μm.

The comparison between PS and toluene suggests that it is the polymeric nature of the medium that affects the nanoparticle size and size distribution. As a result, one might expect that the polymer chain length would affect the particle properties. However, quite surprisingly, we find that the average particle diameter is insensitive to the polymer molecular weight—for over 2 orders of magnitude (approximately 3000–300 000 g/mol), as shown in Figure 1. Thus, controlling particle synthesis via a polymeric matrix does not necessarily require high chain lengths: once some critical molecular weight has been exceeded, the chain molecular weight does not play a role in modulating particle properties.

What is the mechanism by which a homogeneous polymeric environment can control the properties of a growing inorganic nanoparticle population? It is well-known that polymers tend to form adsorbed layers, even

**Table 2. Chemical Structure of the Different Decomposition Media (i.e., Polymeric Matrices) Used in the Synthesis of  $\gamma$ -Fe<sub>2</sub>O<sub>3</sub> Nanoparticles<sup>a</sup>**

Decomposition Medium	Solvent or Polymer Structure	$\phi_{\text{Fe}_2\text{O}_3}$
Toluene		NA
Poly(styrene) (PS)		2.8%
Poly(carbonate) (PC)		6.8%
Poly(Sulfone) (PSF)		2.0%
Poly(methyl methacrylate) (PMMA)		3.2%
Poly(vinylidene difluoride) (PVDF)		4.6%

<sup>a</sup> The volume fraction of iron oxide given in the table applies to the systems shown in Figures 2 and 3.

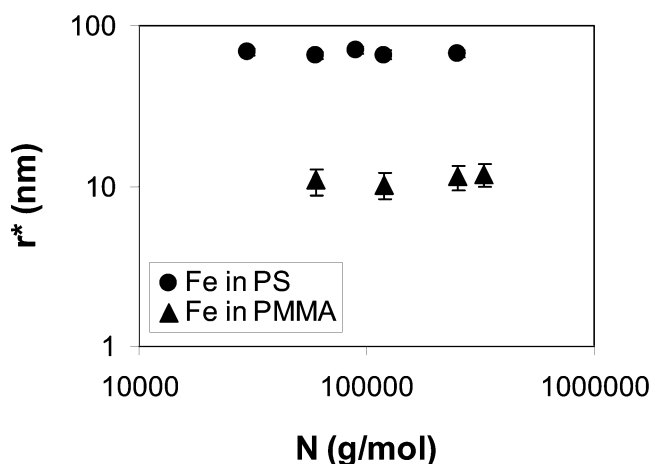


**Figure 1.** Effect of chain molecular weight  $N$  on  $r^*$ , the diameter of equilibrium of  $\gamma$ -Fe<sub>2</sub>O<sub>3</sub> nanoparticles. Two types of polymeric synthesis media are shown: PS (spheres) and PMMA (triangles). The metal volume fraction in PS was 2.8% and in PMMA 3.2%. Error bars for PS are smaller than the marker size. We see that, within the range examined, the equilibrium particle size is independent of the chain length for both types of polymeric matrices.

on weakly attractive substrates where the interaction energy per contact is low.<sup>28</sup> We propose that the adsorbed layer surrounding the growing particle favors an optimal interfacial curvature that sets the equilibrium particle characteristics. Obviously, such a layer would also affect growth kinetics by reducing the rate of metal fragments transport to the growing particle. However, as discussed above, temperature was found to affect the rate of particle formation but not the *equilibrium* particle size.

The free energy of an adsorbed polymer layer is composed of two contributions: the first is due to the chain/particle interaction energy, which favors a thin layer and/or larger particle size. The second contribution arises from the chain deformation energy, which favors thick adsorbed layers whose dimension is similar to the

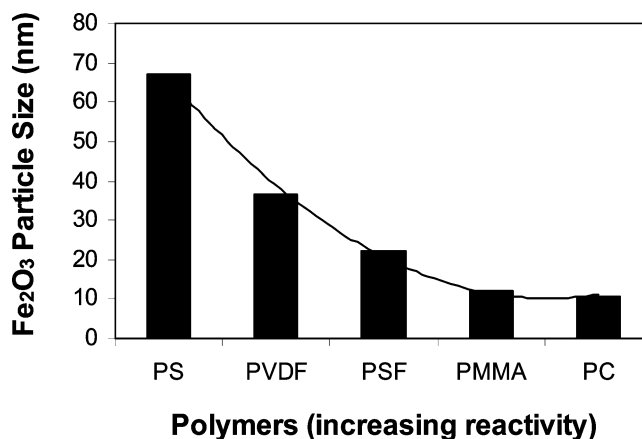


**Figure 2.** Equilibrium diameter of iron oxide nanoparticles synthesized in different polymeric matrices. The polymers are listed in order of increased interactions with the metal: PS/iron oxide surface interactions are the weakest and PC the strongest.<sup>41–45</sup> The volume fraction of the metal for each polymer was relatively low, as listed in Table 1. The average molecular weight of the polymers was 250 000 g/mol for PS, PSF, and PMMA, 300 000 g/mol for PVDF, and 30 000 g/mol for PC. (Note that, as shown in Figure 1, chain molecular weight had no effect on the equilibrium particle size in this MW range.)

chain radius of gyration and/or smaller particle size.<sup>28</sup> In the case of adsorption from a solvent, the mixing energy and entropy between the adsorbed chains and the solvent must be accounted for. However, in this case, the adsorbed chains are similar to the surrounding media, and mixing terms can be neglected. Using a mean-field model to account for these contributions, we find that the equilibrium particle size  $r$  should scale as  $a\{(1/\epsilon - 1)^{1/2} - 1\}$ , where  $a$  is the polymer persistence length and  $(-\epsilon)$  a normalized polymer/particle interaction energy, or surface energy per unit area (the negative sign denotes a net attraction). All coefficients of order unity are neglected. Thus, the model predicts that the particle size is independent of the chain length, in agreement with our data (Figure 1), and that  $r^*$  decreases with increasing strength of the polymer–particle interaction energy.

To examine the effect of the polymer medium chemistry on the iron oxide cluster size, we compare particle formation in several types of polymers, including PS, poly(methyl methacrylate) (PMMA), bisphenol polycarbonate (PC), poly(vinylidene difluoride) (PVDF), and polysulfone (PSF). These polymers span a variety of functional groups that differ in the strength and nature of their interactions with the iron oxide particles and in their position along the polymer chain, either in the main chain or on a side chain (Table 1). As shown in Figure 2, we find that the characteristic nanoparticle size decreases with increasing affinity (i.e., strength of interaction) between the polymer and the iron oxide particles. The qualitative assessment of the chemical affinity between the surfaces of the iron oxide nanoparticles and the functional groups in the various polymers is based on the extensive catalysis literature concerning the reactivity and the molecular mechanisms of interactions between small organic molecules and metal oxide surfaces.<sup>31–42</sup> When polymers are brought into contact with metal oxide nanoclusters, the chemical reactions should be similar if not identical to those of their small molecule counterparts with continuous surfaces, and hence, much can be learned from these latter systems



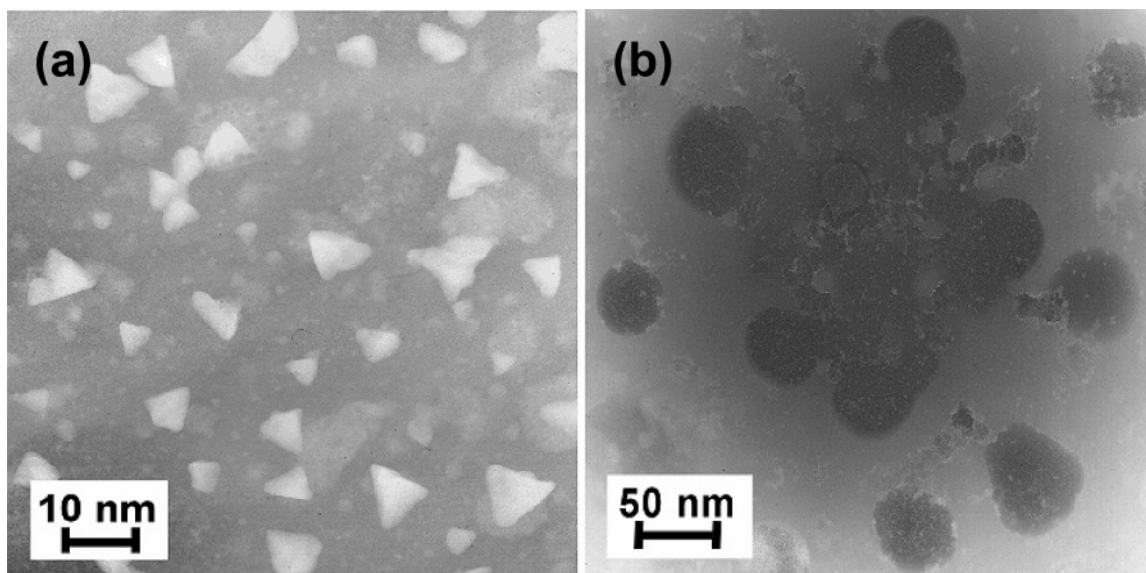


**Figure 3.** Transmission electron micrographs (TEM) of  $\gamma$ - $\text{Fe}_2\text{O}_3$  particles formed in (a) PMMA ( $\bar{M}_w = 250\,000$  g/mol and  $\phi_{\text{Fe}_2\text{O}_3} = 3.2\%$ ) and (b) PS ( $\bar{M}_w = 250\,000$  g/mol and  $\phi_{\text{Fe}_2\text{O}_3} = 2.8\%$ ). Micrographs were taken using both the direct deposition of sample on TEM grids and microtoming the free-standing films, as discussed in the text. Images shown here were obtained by the second method. Scale bars are as labeled. We see that the iron oxide particles in PMMA are smaller than those in PS, and their shape is pyramidal rather than spherical. Note that in both cases the particles seem to be relatively uniform in size and evenly dispersed throughout the polymer matrix.

regarding fundamental aspects of adhesion interactions.<sup>43–47</sup> Therefore, in the particular systems studied here, the order of the extent of interaction with the iron oxide nanoclusters is as follows:  $\text{PC} \geq \text{PMMA} > \text{PSF} > \text{PVDF} > \text{PS}$ .

Particle size in the weakly interacting PS is relatively large ( $\sim 67$  nm) when compared to the  $\sim 10$  nm particles formed in strongly interacting matrices such as PC and PMMA. This is in agreement with the simple model presented here. Another interesting feature is the fact that the polydispersity in particle size was extremely low in all cases, ranging from 4 nm in PS to 2 nm in PMMA and PC.

The interactions between the polymeric medium and the growing metal nanoparticles also control the particle morphology. In a weakly interacting medium, the polymer does not favor any particular crystallographic facet, so the particles grow uniformly in all directions, generating, at equilibrium, spherical objects. In strongly interacting media, growth is inhibited at the polymeric anchor points so that the particle growth is nonuniform.<sup>48,49</sup> Indeed, in Figure 3 we find that particles synthesized in the weakly interacting PS are spherical, while those formed in the strongly interacting PMMA are pyramidal. It is interesting to note that in both polymers the particles seem to be homogeneously distributed throughout the polymeric matrix. Particle volume fraction was kept relatively low in order to optimize particle distribution homogeneity and interparticle distance.

Our model also predicts that the equilibrium particle size is independent of the metal volume fraction in the polymer matrix ( $\phi$ ). Figure 4a we plot the average particle size as a function of  $\phi$  for particles formed in PS and in PMMA. We find that the size of particles in PS is, indeed, independent of the metal volume fraction up to  $\phi \approx 7\%$ . However, the particle size in PMMA remains constant only until  $\phi \approx 4\%$ , above which it increases rapidly. What could explain this uptake? Figure 4b suggests an answer: in this micrograph, we

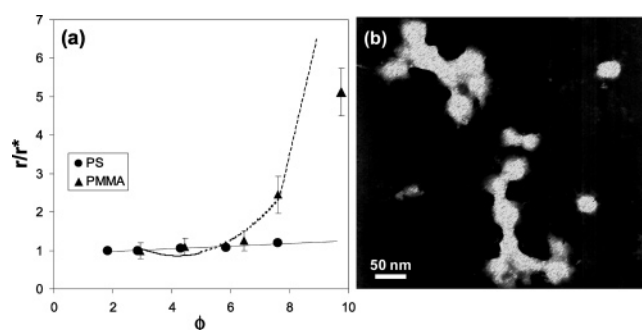


**Figure 4.** (a) Effect of metal volume fraction on particle size in PS (spheres) and PMMA (triangles).  $\bar{M}_w = 250\,000$  g/mol for both polymers in this case. Particle radii were normalized by the equilibrium size in the limit of low volume fraction. The dashed lines were calculated by our model: we first estimated the ratio of interaction energy ( $\epsilon_{\text{PS}}/\epsilon_{\text{PMMA}}$ ) in PS and PMMA required to produce the appropriate equilibrium diameters ratio ( $r_{\text{PS}}^*/r_{\text{PMMA}}^* \approx 65/12$ ), assuming that the Hamaker constant is similar in both polymeric matrices. This ratio was used to calculate the ratio of the critical volume fractions for flocculation ( $\phi_c$ ) for the two polymers. Above the critical volume fraction, average particle size was estimated using the Boltzmann distribution:  $r \sim \phi e^{-p(\phi)/kT}$ . (b) An example of the phenomenon leading to the onset of flocculation is shown in the transmission electron micrographs (TEM) of  $\text{Fe}_2\text{O}_3$  particles formed in PVDF ( $\bar{M}_w = 279\,000$  g/mol,  $\phi_{\text{Fe}_2\text{O}_3} = 4.6\%$ ). We see the initiation of a fractal-like flocculate composed of uniform particles whose diameter is of order 30 nm—the value obtained in the limit of low volume fraction. As expected from our model, particles in PVDF initiate flocculation at a volume fraction that is lower than that of PS (approximately 8%) and higher than that of PMMA (approximately 4%).

see stable particles of relatively uniform size, in this case in a PVDF matrix, that are starting to form a fractal-like flocculate. Indeed, it is reasonable to expect that, as the metal (and thus particle) volume fraction increases, so would the probability for flocculation. However, is it likely that smaller particles formed in the strongly interacting PMMA will flocculate at lower volume fractions than the larger particles formed in the weakly interacting PS?

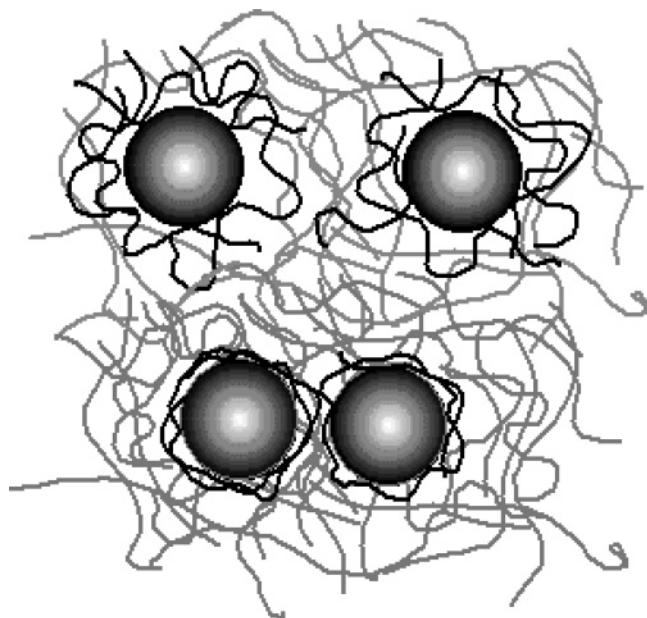


**Figure 5.** A schematic describing the effect of particle/polymer interaction on stability. Adsorbed chains (i.e., those adhering to the nanoparticle surface) are in black, and nonadsorbed chains are in gray. Note that, since the particles are formed in the polymeric matrix, there is interpenetration between adsorbed and nonadsorbed chains in the layer. Attractive van der Waals forces scale as  $1/D^2$ , where  $D$  is the separation between the particle edges. So do, roughly, the repulsive steric forces due to compression of the adsorbed polymer layer. Strongly adsorbed layers (bottom) form a thin layer, which provides strong repulsion—but only when the particles are relatively close and the van der Waals interaction may be strong. Weakly adsorbed layers provide weak repulsion—but at larger particle–particle separations where van der Waals attraction is negligible.

Particle flocculation is induced by ubiquitous, attractive particle–particle van der Waals interactions. In our system, these are balanced by a steric repulsion between the polymer layers surrounding the particle. Our mean field model predicts that flocculation will occur once the metal volume fraction increases above a critical value. The critical volume fraction for flocculation ( $\phi_c$ ) is found to vary as a function of the particle–polymer interaction energy, scaling, in the limit of high chain molecular weight, as  $\exp[AN\{\epsilon(1/\epsilon - 1)^{1/2} - 1\}/\{(2/\epsilon - 1)^{1/2} - 1\}]$ , where  $A$  is the Hamaker constant and  $N$  the chain molecular weight.<sup>28,50</sup>

The model therefore predicts that the critical volume fraction for flocculation will decrease with increasing particle–polymer interaction. As a result, flocculation in the strongly interacting PMMA should occur at lower volume fractions than in the weakly interacting PS, in agreement with the data presented in Figure 4a. Also, it should be noted that, unlike the equilibrium nanoparticle diameter, the critical flocculation volume fraction increases sharply with the polymer chain molecular weight. Flocculation may be inhibited by increasing the matrix molecular weight, without affecting the properties of the individual particles.

Why do weakly interacting polymers stabilize particles better than strongly interacting ones? This is due to the fact that the strength of the steric repulsion increases with increasing chain density on the surface, while its range is set by the adsorbed layer thickness, as shown schematically in Figure 5. Since the adsorbed layer thickness decreases, and the density increases,

with increasing polymer/particle affinity,<sup>28</sup> in weakly interacting media the adsorbed polymer layer provides long-range, weak repulsion. On the other hand, in strongly interacting media the repulsion is short range and strong, van der Waals interactions are weak at long range and strong at short range, so that stabilization against flocculation is more sensitive to the range of the repulsive force than its strength. Thus, weakly adsorbed layers will stabilize particles against flocculation more effectively than strongly interacting polymers.

#### 4. Summary

In conclusion, we present here a method for the controlled synthesis of inorganic nanoparticles in a uniform polymeric environment. We show that the particle size, size distribution, and morphology may be controlled through the type of polymer used; strongly interacting matrices produce smaller particles with a nonspherical morphology, while weakly interacting media lead to larger spherical particles. However, in all cases, the polydispersity was shown to be low, in contrast to nonpolymeric small molecule media where the distribution is relatively wide even when the interfacial interactions are favorable. The fact that particle size is independent of the chain length means that choice of the matrix molecular weight can be set by processing requirements and will not affect the inorganic particle properties. Also, particle size remains independent of the inorganic volume fraction up to a critical value, which decreases with increasing polymer–particle interfacial interactions. Below this critical value, the nanoparticles are uniformly distributed throughout the polymeric matrix, while above it they form larger flocculates. Therefore, it is possible to produce nanocomposites of similar particle properties but different inorganic content.

The ability to select nanoparticle properties through their interactions with a polymeric matrix is not limited to iron oxide or even to other metal chemistries. Understanding the mechanism by which the polymer matrix sets the nanoparticle size can be used to extend the method to a variety of inorganic systems, thereby enabling the formation of uniform nanoparticles and nanocomposites with predesigned characteristics.

**Acknowledgment.** This work was funded by DARPA and the Air Force Research Labs/MLBP/WPAFB, Contract F33615-01-C-5023, and by the American Chemical Society, Petroleum Research Fund, PRF 40014-AC5M. N.D. acknowledges partial support by an NSF-NIRT Grant 0304453.

#### References and Notes

- (1) Edelstein, A. S.; Cammarata, R. C. Eds.; *Nanomaterials: Synthesis, Properties and Applications*; Inst. Phys. Publishing: London, UK, 1996.
- (2) Service, R. F. *Science* **1996**, *271*, 920.
- (3) Cheng, C. C.; Arbet-Engels, V.; Scherer, A.; Yablonovitch, E. *Phys. Scr.* **1996**, *T68*, 17.
- (4) Wijnhoven, J. E. G. J.; Vos, W. L. *Science* **1998**, *281*, 802.
- (5) Summers, C. J.; Neff, C. W.; Park, W. J. *Nonlinear Opt. Phys. Mater.* **2003**, *12*, 587.
- (6) Sun, Y. G.; Xia, Y. N. *Science* **2002**, *298*, 2176.
- (7) Seifert, G. *Nat. Mater.* **2004**, *3*, 77.
- (8) Weiner, S.; Addadi, L. *Trends Biochem. Sci.* **1991**, *16*, 252.
- (9) Nys, Y.; Hincke, M. T.; Arias, J. L.; Gracia-Ruiz, J. M.; Solomon, S. E. *Poultry Avian Bio. Rev.* **1999**, *10*, 143–166.
- (10) Fernandez, M. S.; Moya, A.; Lopez, L.; Aria, J. L. *Matrix Biol.* **2001**, *19*, 793.

- (11) Pitcher, M. W.; Cates, E.; Raboin, L.; Bianconi, P. A. *Chem. Mater.* **2000**, *12*, 1738.
- (12) Gubin, S. P. *Colloids Surf. A* **2002**, *202*, 155.
- (13) Jolivet, J. P.; Tronc, E.; Chaneac, C. *Eur. Phys. J. Appl. Phys.* **2000**, *10*, 167.
- (14) Vayssières, L.; Chanéac, C.; Tronc, E.; Jolivet, J.-P. *J. Colloid Interface Sci.* **1998**, *205*, 205.
- (15) Mendoza-Resendez, R.; Morales, M. P.; Serna, C. J. *Mater. Sci. Eng., C* **2003**, *23*, 1139.
- (16) Berry, C. C.; Curtis, A. S. G. *J. Phys. D: Appl. Phys.* **2003**, *36*, R198.
- (17) Gupta, A. K.; Curtis, A. S. G. *Biomaterials* **2004**, *25*, 3029.
- (18) Ennas, G.; Musinu, A.; Piccaluga, G.; Zedda, D.; Gatteschi, D.; Sangregorio, C.; J. Stanger, L.; Concas, G.; Spano, G. *Chem. Mater.* **1998**, *10*, 495.
- (19) Moreno, E. M.; Zayat, M.; Morales, M. P.; Serna, C. J.; Roig, A.; Levy, D. *Langmuir* **2002**, *18*, 4972.
- (20) Cannas, C.; Concas, G.; Gatteschi, D.; Musinu, A.; Piccaluga, G.; Sangregorio, C. *J. Mater. Chem.* **2002**, *12*, 3141.
- (21) Chhabra, V.; Ayyub, P.; Chattopadhyay, S.; Maitra, A. N. *Mater. Lett.* **1996**, *26*, 21.
- (22) Tartaj, P.; Serna, C. J. *Chem. Mater.* **2002**, *14*, 4396.
- (23) Zhang, L.; Papaefthymiou, G. C.; Ying, J. Y. *J. Phys. Chem. B* **2001**, *105*, 7414.
- (24) Tannenbaum, R.; Flenniken, C. L.; Goldberg, E. P. *J. Polym. Sci., Part B: Polym. Phys. Ed.* **1990**, *28*, 2421.
- (25) Tadd, E. H.; Zeno, A.; Zubris, M.; Dan, N.; Tannenbaum, R. *Macromolecules* **2003**, *36*, 6497.
- (26) King, S.; Hyunh, K.; Tannenbaum, R. *J. Phys. Chem. B* **2003**, *107*, 12097.
- (27) deGennes, P. G. *Scaling Concepts in Polymer Physics*; Cornell University Press: Ithaca, NY, 1979.
- (28) Netz, R. R.; Andelman, D. *Phys. Rep.* **2003**, *380*, 1.
- (29) Israelachvili, J. N. *Intermolecular and Surface Forces: With Applications to Colloidal and Biological Systems*; Academic Press: New York, 1985.
- (30) Kimata, M.; Nakagawa, D.; Hasegawa, M. *Powder Technol.* **2003**, *132*, 112.
- (31) Crispin, X.; Lazzaroni, R.; Geskin, V.; Baute, N.; Dubois, P.; Jerome, R.; Bredas, J. L. *J. Am. Chem. Soc.* **1999**, *121*, 176.
- (32) Karpovich, D. S.; Blanchard, G. *J. Langmuir* **1997**, *13*, 4031.
- (33) Barlow, S. M.; Raval, R. *Surf. Sci. Rep.* **2003**, *50*, 141.
- (34) Bizzotto, D. *Electrochem. Soc. Interface* **1996**, *5*, 47.
- (35) King, E. M.; Clark, S. J.; Verdozzi, C. F.; Ackland, G. J. *J. Phys. Chem. B* **2001**, *105*, 641.
- (36) Sasaki, M.; Yoshida, S. *Appl. Surf. Sci.* **1997**, *121–122*, 73.
- (37) Ehara, T.; Hirose, H.; Kobayashi, H.; Kotani, M. *Synth. Met.* **2000**, *109*, 43.
- (38) Johansson, E.; Nyborg, L. *Surf. Interface Anal.* **2000**, *30*, 333.
- (39) Losic, D.; Shapter, J. G.; Gooding, J. J. *Langmuir* **2002**, *18*, 5422.
- (40) Zou, S.; Williams, C. T.; Chen, E. K.-Y.; Weaver, M. J. *J. Phys. Chem. B* **1998**, *102*, 9039.
- (41) Barlow, S. M.; Haq, S.; Raval, R. *Langmuir* **2001**, *17*, 3292.
- (42) Zhao, H.; Kim, J.; Koel, B. E. *Surf. Sci.* **2003**, *538*, 147.
- (43) Cai, L.; Xiao, X.; Loy, M. M. T. *Surf. Sci.* **2001**, *492*, L688.
- (44) Zubkov, T.; Morgan Jr., G. A.; Yates, J. T., Jr.; Kuhlert, O.; Lisowski, M.; Schillinger, R.; Fick, D.; Jansch, H. *J. Surf. Sci.* **2003**, *526*, 57.
- (45) Rzeznicka, I. I.; Matsushima, T. *J. Phys. Chem. B* **2003**, *107*, 8479.
- (46) Ormerod, R. M.; Lambert, R. M.; Bennett, D. W.; Tysoe, W. T. *Surf. Sci.* **1995**, *330*, 1.
- (47) Carrez, S.; Dragnea, B.; Zheng, W. Q.; Dubost, H.; Bourguignon, B. *Surf. Sci.* **1999**, *440*, 151.
- (48) Yu, S. H.; Colfen, H.; Antonietti, M. *Chem.—Eur. J.* **2002**, *8*, 2937.
- (49) Bronstein, L. M.; Linton, C.; Karlinsey, R.; Stein, B.; Timofeeva, G. I.; Svergun, D. L.; Konarev, P. I.; Kozin, M.; Tomaszewski, J.; Werner-Zwanziger, U.; Zwanziger, J. W. *Langmuir* **2004**, *20*, 1100.
- (50) Aubouy, M.; Raphael, E. *Macromolecules* **1998**, *31*, 4357.

MA048317X